Organic & Biomolecular Chemistry

Cite this: *Org. Biomol. Chem.*, 2012, **10**, 7037

www.rsc.org/obc

PAPER

New insights into the mechanism of the Schiff base hydrolysis catalyzed by type I dehydroquinate dehydratase from *S. enterica*: a theoretical study

Yuan Yao*[a,b] and Ze-Sheng Li*[c,b]

Received 22nd March 2012, Accepted 4th July 2012
DOI: 10.1039/c2ob25605c

The reaction pathway of Schiff base hydrolysis catalyzed by type I dehydroquinate dehydratase (DHQD) from *S. enterica* has been studied by performing molecular dynamics (MD) simulations and density functional theory (DFT) calculations and the corresponding potential energy profile has also been identified. On the basis of the results, the catalytic hydrolysis process for the wild-type enzyme consists of three major reaction steps, including nucleophilic attack on the carbon atom involved in the carbon–nitrogen double bond of the Schiff base intermediate by a water molecule, deprotonation of the His143 residue, and dissociation between the product and the Lys170 residue of the enzyme. The remarkable difference between this and the previously proposed reaction mechanism is that the second step here, absent in the previously proposed reaction mechanism, plays an important role in facilitating the reaction through a key proton transfer by the His143 residue, resulting in a lower energy barrier. Comparison with our recently reported results on the Schiff base formation and dehydration processes clearly shows that the Schiff base hydrolysis is rate-determining in the overall reaction catalyzed by type I DHQD, consistent with the experimental prediction, and the calculated energy barrier of ~16.0 kcal mol^{-1} is in good agreement with the experimentally derived activation free energy of ~14.3 kcal mol^{-1}. When the imidazole group of His143 residue is missing, the Schiff base hydrolysis is initiated by a hydroxide ion in the solution, rather than a water molecule, and both the reaction mechanism and the kinetics of Schiff base hydrolysis have been remarkably changed, clearly elucidating the catalytic role of the His143 residue in the reaction. The new mechanistic insights obtained here will be valuable for the rational design of high-activity inhibitors of type I DHQD as non-toxic antimicrobials, anti-fungals, and herbicides.

Introduction

The dehydration of dehydroquinate to dehydroshikimate catalyzed by dehydroquinate dehydratase (DHQD), as depicted in Scheme 1, occurs in both the biosynthetic shikimate pathway and the degradative quinate pathway. In the biosynthetic shikimate pathway, DHQD introduces a double bond into the hexane ring of the substrate, which is further converted to be the central metabolite, chorismic acid. As a precursor, a lot of aromatic compounds are made from it including the aromatic amino acids, ubiquinone and vitamin E.[1] The fact that the shikimate pathway is only found in all prokaryotes and in lower eukaryotes such as fungi and plants but not in mammals makes it a potential target for antimicrobial agents and herbicides. In the catabolic pathway, dehydroshikimate is further aromatized to protocatechuic acid that goes on to be metabolized to acetyl-CoA through the β-ketoadipate pathway.[2] This pathway has been found in both fungi and prokaryotes such as *Amylocaptosis methanolica* and *Acinetobacter calcoaceticus*.[3,4]

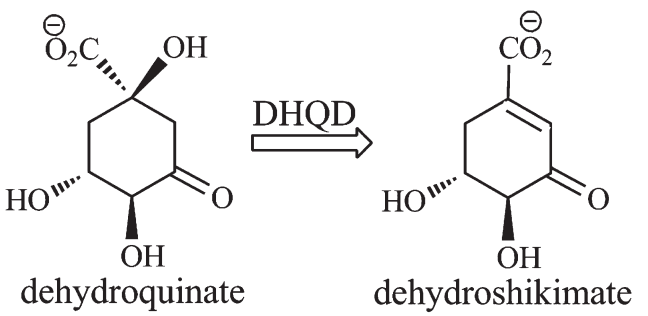

Scheme 1 The dehydration of dehydroquinate to dehydroshikimate catalyzed by dehydroquinate dehydratase (DHQD).

[a]*State Key Laboratory of Urban Water Resource and Environment, Harbin Institute of Technology, Harbin 150090, People's Republic of China. E-mail: yyuan@hit.edu.cn*
[b]*Academy of Fundamental and Interdisciplinary Science, Academy of Science and Industrial Technology, Harbin Institute of Technology, Harbin, 150080, People's Republic of China*
[c]*Key Laboratory of Cluster Science of Ministry of Education & School of Chemistry, Beijing Institute of Technology, Beijing, 100081, People's Republic of China. E-mail: zeshengli@bit.edu.cn; Fax: +86-10-68918670*

Two distinguishable types of DHQD enzymes have been identified, known as type I and type II. Surprisingly, they neither share any sequence similarities, nor employ the same reaction mechanism, but catalyze the same chemical reaction, representing an unusual case of convergent evolution.[5–8] Type I DHQD catalyzes the dehydration of dehydroquinate through a covalent Schiff base intermediate formed between the substrate and Lys170 residue.[7] By contrast, type II DHQD undergoes an enolate intermediate to catalyze the reaction.[7,9] Another remarkable mechanistic difference between these two types of the enzymes is the stereochemistry of the elimination reaction; type I DHQD employs *cis*-elimination,[10] in contrast to *trans*-elimination for type II DHQD.[11] Therefore, it is of great mechanistic and evolutionary interest to explore the structures and mechanisms of DHQDs and understand how this case arises. This may further direct the rational design of inhibitors of type I DHQD as non-toxic antimicrobials, anti-fungals, and herbicides. In the past twenty years, several studies, including chemical modification, mutagenesis, peptide mapping, and protein crystallization, have been conducted on type I DHQD and the results have revealed some features of its reaction mechanism and enzymatic chemistry. It has been proposed that the dehydration of dehydroquinate catalyzed by type I DHQD consists of three reaction stages, including the Schiff base formation, dehydration process, and the Schiff base hydrolysis, and the third stage, the hydrolysis of the Schiff base, might be expected to be the rate-determining step based on the previously proposed reaction mechanism.[12] The Lys170 residue is conserved in all the known type I DHQDs[13–16] and has been identified to form the covalent Schiff base intermediates with the substrate by both chemical modification and peptide mapping studies. The reduction of the intermediates significantly affects the stability of the resulting enzyme,[17,18] which is consistent with the fact that the mutation of K170A results in a $\sim 10^6$-fold reduction in catalytic activity.[12] Another important residue is His143 as the mutation of H143A also results in a $\sim 10^6$-fold reduction in catalytic activity and several experimental results imply that this residue has a wide ranging influence on the mechanism of the enzyme.[12] The His143 residue was proposed to catalyze the dehydration process as a general base and be involved in the formation and hydrolysis of the Schiff base intermediates.[12] In the latter role, His143 was proposed to be a general acid in the Schiff base formation and then a general base in its hydrolysis. This postulation is supported by the recently reported X-ray crystal structures of type I DHQD with pre- and post-dehydration reaction intermediate (PDB codes: 3M7W and 3JS3), which show the His143 residue having a particularly striking reaction state-dependent structural behavior.[19] In the pre-dehydration complex, the His143 residue is proximal to both elements of the catalytic dehydration, where the $N^{\varepsilon 2}$ atom of the His143 residue is located towards the C-2 atom of the substrate and forms a hydrogen bond with the 1-hydroxyl leaving group. In the post-dehydration complex, the side chain of the His143 residue is displaced ~1.5 Å away from the site in the pre-dehydration complex to the position that is adopted in all previously reported apo and post-dehydration reaction intermediate structures.[6,20–22] However, the detailed reaction mechanism of the dehydration of dehydroquinate catalyzed by type I DHQD and the catalytic roles of Lys170 and His143 residues remain unclear.

To understand the fundamental reaction mechanism for the dehydration of dehydroquinate catalyzed by type I DHQD, we have carried out several computational studies on type I DHQD from *S. enterica* interacting with dehydroquinate[23,24] in comparison with available experimental results. According to our computational results, the Schiff base formation consists of four reaction steps with the energy barrier of ~12.1 kcal mol^{-1}, different from the proposed reaction pathway which has been verified to have an unfavorable energy barrier of ~30.7 kcal mol^{-1}. The His143 residue plays a more complicated role in this process, in that it deprotonates the Lys170 residue before the substrate binding and facilitates the formation of the Schiff base intermediate through mediating two proton transfers in the reaction. The dehydration process undergoes a two-step *cis*-elimination reaction mechanism with an energy barrier of ~6.4 kcal mol^{-1}. The proposed carbanion intermediate cannot be identified because of its low stabilization. During this process, the His143 residue acts as a general base to accept the H_R proton from the C_2 position of the substrate. However, it should be pointed out that the detailed reaction mechanism of the hydrolysis of Schiff base intermediate has not been reported so far, and there have been no complete studies on the overall dehydration reaction of dehydroquinate catalyzed by type I DHQD from *S. enterica*.

In the present study, the fundamental reaction mechanism for the Schiff base hydrolysis catalyzed by type I DHQD from *S. enterica* was investigated by performing MD simulation and quantum chemical calculations and the catalytic role of His143 during this process was also elucidated. By comparison with our recent studies on the Schiff base formation and dehydration process, the rate-determining step for the overall reaction was identified. On the basis of our results, future efforts aiming at the design of high activity inhibitors for the enzyme were suggested.

Computational details

Structure preparation

The starting model of the system was based on the crystal structure of type I DHQD with pre-dehydration Schiff base intermediate (PDB code 3M7W). In MD simulation performed by AMBER 9 package,[25,26] the system was solvated in a rectangular box of TIP3P water molecules[27] with a minimum solute-wall distance of 10 Å. It was gradually heated from 10 K to 298.15 K over 50 ps before running ~2 ns MD simulation at 298.15 K. The time step was set as 2 fs. The SHAKE algorithm[28,29] was used to fix all covalent bonds containing hydrogen atoms. The particle mesh Ewald (PME) method was used to treat long-range electrostatic interactions. In the present study, a snapshot close to the average structure from the MD simulation was used to prepare the model for quantum chemical calculations.

Quantum chemical calculations

All quantum chemical calculations presented here were performed using the density functional theory (DFT) B3LYP as implemented in Gaussian 03 program.[30] For geometry optimization, the 6-31G* basis set was used and the initial geometry coordinates of the stationary points were set for the geometry

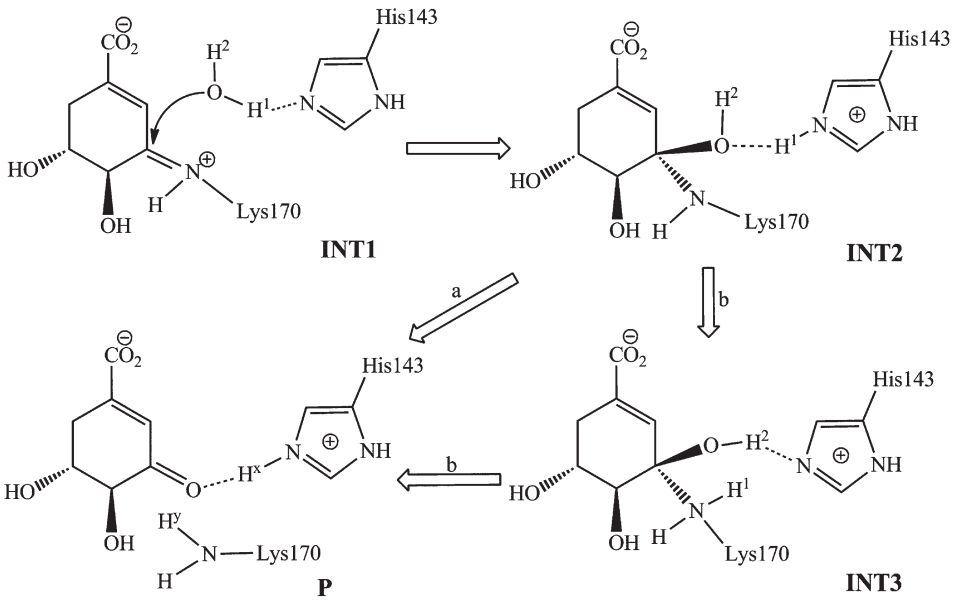

Scheme 2 The previously proposed reaction pathway (labeled by a) and the currently elucidated reaction pathway (labeled by b) for the Schiff base hydrolysis catalyzed by type I DHQD. For the product in the proposed reaction pathway, $x = 1$ and $y = 2$. For that in the currently elucidated reaction pathway, $x = 2$ and $y = 1$.

optimization on the basis of the reaction coordinates involved in the reaction mechanism shown in Scheme 2. Once the optimization was done, a frequency calculation followed to identify the nature of the stationary point. During the geometry optimizations, the truncated atoms were fixed to prevent unrealistic movements of the various groups in the models. This technology resulted in a few small imaginary frequencies, which can be ignored because they do not contribute significantly to the energy. In order to obtain more accurate energy, single-point calculations based on the optimized geometries were carried out using B3LYP/6-311+G(2d,2p) level and the zero-point and thermal corrections were also taken into account. The solvent effects were calculated at the same level as the geometry optimization by performing single-point calculations on the optimized geometries using the polarizable continuum model (PCM) method[31–33] with the dielectric constant of 4, which is suitable and widely used to mimic the protein environment.[34] The computational method, the basis set, and the relative parameters here have been successfully used to study the enzymatic reaction mechanism through quantum chemical model and the results are reasonable and reliable.[35–44]

Results and discussion

Identification of the nucleophilic water molecule

It was proposed that the Schiff base hydrolysis catalyzed by type I DHQD was initialized by a water molecule and that it behaves as a nucleophile, attacking the C_3 atom involved in the carbon–nitrogen double bond of the Schiff base intermediate[12] as shown in Scheme 2. This water molecule needs to be close enough to the C_3 atom to initiate the nucleophilic attack process. However, no such water molecule was observed in the initially modeled structure. It is necessary to identify a nucleophilic water molecule before quantum chemical calculations. Thus, the MD

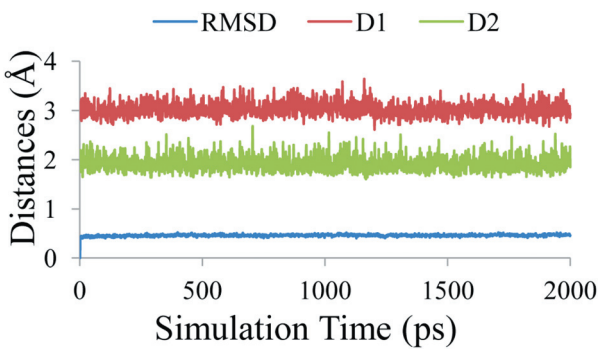

Fig. 1 Key internuclear distances *vs.* simulation time in MD simulation.

simulation was performed on the system to identify the water molecule. A ~2 ns simulation should be adequate in sampling the water molecule. As shown in Fig. 1, the time-dependent RMSD curve to track the Cα atoms in the enzyme did not significantly change, meaning that the enzyme is very stable during the simulation. By analyzing the trajectory, we observed a solvent water molecule located close to the C_3 atom and His143 residue. It forms a strong hydrogen bond with the $N^{\varepsilon 2}$ atom of the His143 residue. The simulated key distances associated with this crucial water molecule, including the distance (D1) between the water oxygen atom and C_3 atom as well as the distance (D2) between the H^1 atom of the water molecule and the $N^{\varepsilon 2}$ atom of the His143 residue, are also shown in Fig. 1 and these key distances were very stable during the simulation. The average values of D1 and D2 reveal that this water molecule was in an appropriate position to attack the C_3 atom. On the basis of the structural information above, this water molecule was identified to be the nucleophile to initiate the hydrolysis process of Schiff base intermediate.

Fundamental reaction pathway

On the basis of the selected snapshot from the MD simulation, a quantum chemical model was constructed and it consists of the post-dehydration Schiff base intermediate and the side chains of the other seven active site residues. From this model, the fundamental reaction pathway for the Schiff base hydrolysis catalyzed by type I DHQD has been revealed by performing DFT calculations and the relative potential energy profile has also been identified. The results indicate that the hydrolysis reaction consists of three reaction steps (shown in Scheme 2), including the nucleophilic attack on the C_3 atom involved in the carbon–nitrogen double bond of the Schiff base intermediate by water, the deprotonation of the His143 residue, and finally the dissociation between the product and Lys170 of the enzyme. Evidently, this pathway is different from the previously proposed one. Below we discuss each step in detail.

Step 1: the nucleophilic attack on the C_3 atom in the Schiff base intermediate by a water molecule. The nucleophilic attack proceeds as the water oxygen atom gradually approaches the C_3 atom in the Schiff base intermediate. Meanwhile, the H^1 proton in the water molecule gradually moves toward the $N^{\varepsilon 2}$ atom of the His143 residue. The optimized geometries of intermediates and transition state in this step are shown in Fig. 2. As shown in Fig. 2, the water molecule is located close to the C_3 atom of the Schiff base intermediate with a distance between the C_3 atom and the water oxygen atom of 3.34 Å in **INT1**. Moreover, this water molecule forms a strong hydrogen bond with the His143 residue, with a distance between the H^1 atom in water molecule and the $N^{\varepsilon 2}$ atom of His143 residue of 1.73 Å. This is suitable for the His143 residue to accept the proton from the water molecule as a general base. While the water oxygen atom gradually approaches the C_3 atom, through a transition state **TS1**, the geometry of **INT1**, in which the C_3 atom is sp^2 hybridized and is in a planar geometry with its three bonding atoms, gradually changes to be an sp^3 hybridized C_3 atom with a tetrahedral geometry in **INT2**. In **INT2**, the distances between the water oxygen atom and the C_3 atom, or the H^1 atom are 1.49 and 1.71 Å, respectively, showing the finish of both the nucleophilic attack and the proton transfer from the water molecule to the His143 residue. The His143 residue is protonated in **INT2**.

Step 2: the deprotonation of the His143 residue. The deprotonation of the His143 residue proceeds as the proton in the His143 residue gradually transfers to the NZ atom of the Schiff base intermediate. The optimized geometries of the transition state and intermediate in this step are shown in Fig. 3. As shown in Fig. 3, through a transition state of **TS2**, the H^1 proton in the His143 residue has been transferred to the NZ atom of the Schiff base intermediate and the His143 residue is deprotonated in **INT3** as **INT1**. Meanwhile, the 3-hydroxyl group gradually rotates toward the $N^{\varepsilon 2}$ atom of the His143 residue and a strong hydrogen bond is formed between them with a distance of 1.67 Å in **INT3**.

Step 3: the dissociation between the product and the Lys170 residue. The dissociation between the product, dehydroshikimate, and the Lys170 residue proceeds as the C–N bond in the Schiff base intermediate gradually breaks. Meanwhile, the

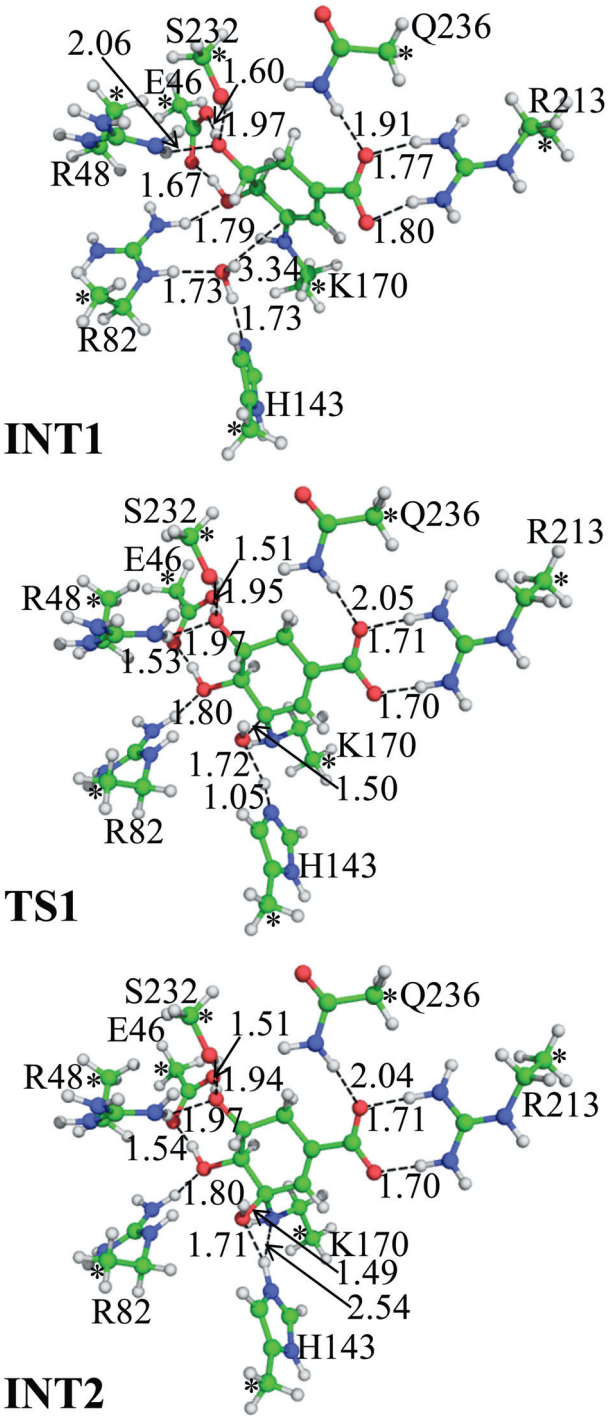

Fig. 2 The optimized geometries in the first reaction step in the reaction of the wild-type enzyme. The distances are in angstrom. Carbon, oxygen, nitrogen, and hydrogen atoms are colored in green, red, blue, and white, respectively. The carbon atoms labeled by an asterisk are fixed during the optimization. Fig. 3 below is represented in the same way.

H^2 proton of the 3-hydroxyl group gradually transfers to the $N^{\varepsilon 2}$ atom of the His143 residue. The optimized geometries of transition state and intermediate in this step are also shown in Fig. 3. As shown in Fig. 3, the geometry of **INT3**, in which the C_3 atom is sp^3 hybridized and is in a tetrahedral geometry, gradually

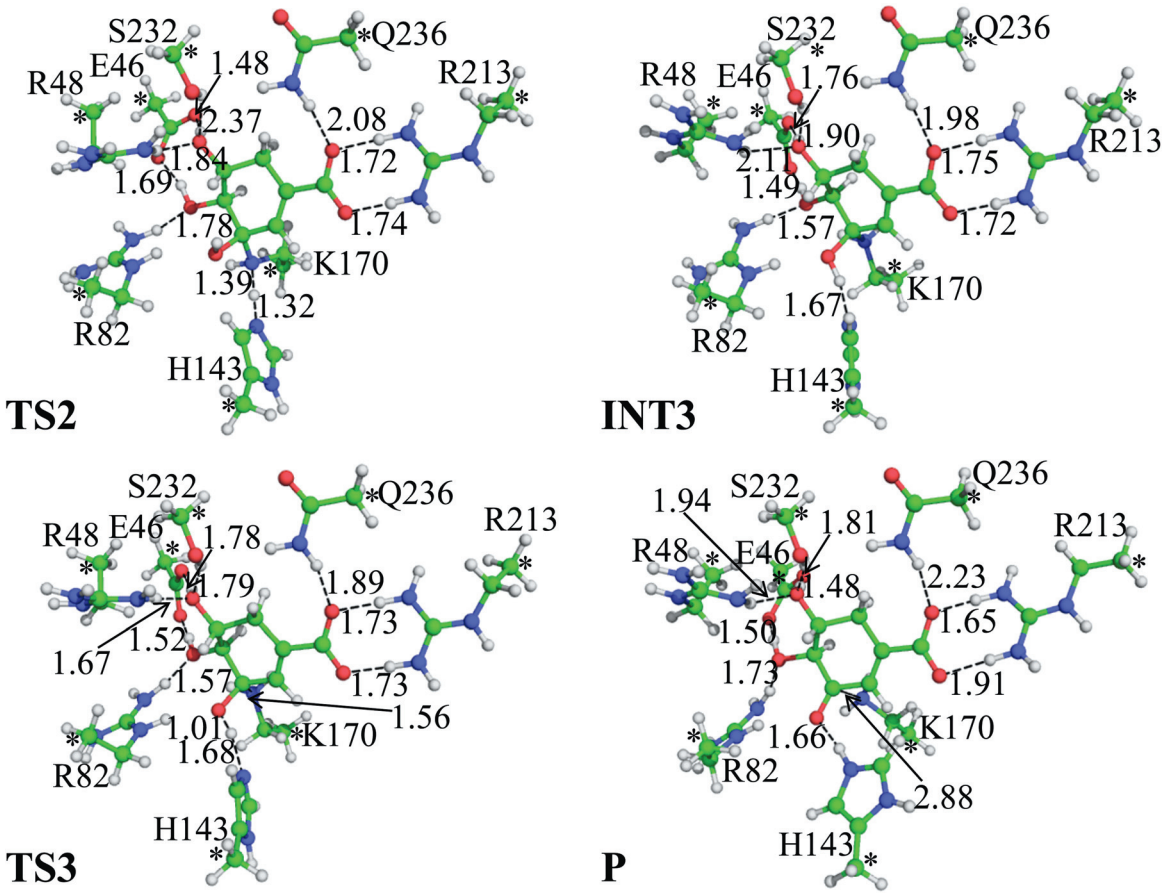

Fig. 3 The optimized geometries in the second and third reaction steps in the reaction of the wild-type enzyme.

changes to be a planar geometry with an sp^2 hybridized C_3 atom in **P** through the transition state **TS3**. The distance between the C_3 atom and the NZ atom of Lys170 is elongated to be 2.88 Å in **P**, showing the complete breaking of the covalent bond between the product and Lys170 residue. In addition, the distance between the O and H^2 atoms in the 3-hydroxyl group is also elongated to be 1.66 Å in **P**, showing the completion of the proton transfer to the His143 residue from the 3-hydroxyl group. Finally, the product dehydroshikimate is released.

Energetics

Using the optimized geometries at B3LYP/6-31G* level, we carried out single-point energy calculations at B3LYP/6-311+G (2d, 2p) level and the zero-point and thermal corrections for each stationary points along the reaction pathway to get more accurate energy, and the solvent effects were evaluated at the same level as the geometry optimization by performing single-point calculations on the optimized geometries using the polarizable continuum model (PCM) method with the dielectric constant of 4. Depicted in Fig. 4 is the energy profile of the hydrolysis of the Schiff base intermediate. As shown in Fig. 4, **INT2** has higher energy than **INT1**, and the energy of **TS2** is also higher than that of **TS1**, showing that the overall energy barrier of the hydrolysis of the Schiff base intermediate is the energy difference between **TS2** and **INT1**, which is calculated to be

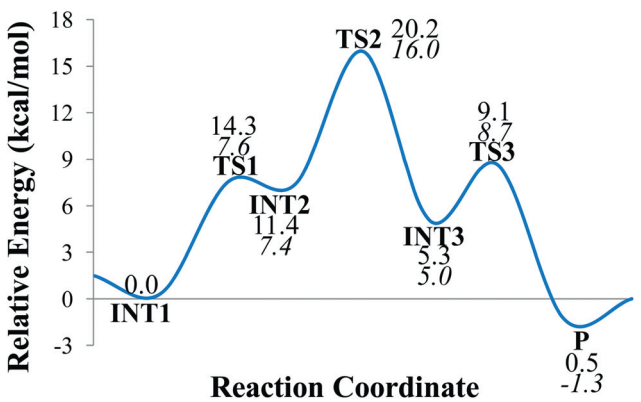

Fig. 4 The potential energy profile of the Schiff base hydrolysis catalyzed by type I DHQD. The energies calculated in enzymatic environment are given in italic type.

~16.0 kcal mol^{-1} in enzymatic environment. By comparing with the calculated energy barriers for the formation of the Schiff base intermediate and the dehydration process of 12.1 kcal mol^{-1} and 6.4 kcal mol^{-1}, it can be concluded that the hydrolysis of the Schiff base intermediate is the rate-determining step as it has the highest energy barrier, which confirms the prediction on the basis of the kinetics study of H143A[12] that the hydrolysis of the Schiff base intermediate is rate-determining. In quantity, the calculated energy barrier of the rate-determining step of

16.0 kcal mol^{-1} is in good agreement with the activation free energy of ~14.3 kcal mol^{-1} derived from the experimental rate constant (K_{cat} = 210 s^{-1})[19] by using the conventional transition state theory (CTST).[45,46]

Comparison between the two reaction mechanisms

As shown in Scheme 2, the currently elucidated reaction mechanism for the hydrolysis of the Schiff base intermediate has the same first step as the previously proposed one. However, the following steps are different. To better understand the detailed mechanism, it is interesting to analyze the difference between them. For the second step in the previously proposed reaction mechanism, the H^2 proton in the 3-hydroxyl group is directly transferred to the NZ atom of the Lys170 residue to facilitate the dissociation between the product and Lys170 residue. By contrast, in the currently elucidated reaction mechanism, the H^2 proton in the 3-hydroxyl group is transferred to the His143 residue in the third reaction step after the H^1 proton transfer from the His143 residue to the Lys170 residue in the second step. By checking the optimized geometry of **INT2**, one can see that the H^2 proton, 3-hydroxyl oxygen atom, and the NZ atom in the Schiff base intermediate are located with an angle between them of 140.9° and a distance between the H^2 proton and the NZ atom of 3.12 Å. These conformational features show that the H^2 proton is located in an unsuitable position for the direct transfer to the NZ atom in the Schiff base intermediate and this may result in a very high energy barrier, like the previously proposed reaction mechanism for the formation of the Schiff base intermediate in our recent study.[24] In the currently elucidated reaction mechanism, this problem is successfully avoided through the deprotonation of the His143 residue in the second step. This process not only protonates the amine group of the Schiff base intermediate, but also makes the His143 residue be deprotonated and further accept the proton from the 3-hydroxyl group. Evidently, these two proton transfers are more favorable than the direct H^2 proton transfer from the 3-hydroxyl group to the Lys170 residue.

The role of the catalytic His143 residue

His143 was proposed to play an important role in the reaction and the H143A mutation has been reported to have a significant influence on the Schiff base hydrolysis.[12] In order to exactly explore the catalytic role of the His143 residue, the Schiff base hydrolysis catalyzed by the H143A mutant has also been studied by performing MD simulation and quantum chemical calculations. The result of the MD simulation indicates that no water molecule can stably locate a suitable position for the nucleophilic attack on the C_3 atom of the Schiff base intermediate. By checking the active site of the mutant, one can see that there is no residue around the Schiff base intermediate to act as a general base just like the His143 residue does. Without the involvement of a general base, it should be very hard for a water molecule to perform nucleophilic attack on the C_3 atom of the Schiff base intermediate. A possible nucleophile to initiate the Schiff base hydrolysis would be hydroxide ion in the solution because of its stronger nucleophilic property. Thus, the reaction mechanism of Schiff base hydrolysis of the H143A mutant initiated by hydroxide ion was studied by performing quantum chemical calculations. When we tried to optimize the transition state for nucleophilic attack on the C_3 atom by hydroxide ion, the covalent bond between the C_3 atom and the hydroxide ion always forms with the bond length of 1.46 Å which is the relevant value in **INT2$_{H143A}$**, even though we set the distance between the C_3 atom and the hydroxide ion as long as 4.0 Å in the initial coordinate. This process therefore is scanned and the result shows a barrierless nucleophilic attack. In **INT2$_{H143A}$**, the distance between the NZ atom in the Lys170 residue and the H atom of the 3-hydroxyl group is 2.31 Å, suitable for direct proton transfer. Through **TS2$_{H143A}$** with a four-membered ring conformation, the covalent bond between the product and the Lys170 residue breaks. As depicted in Fig. 5 and 6, overall, this

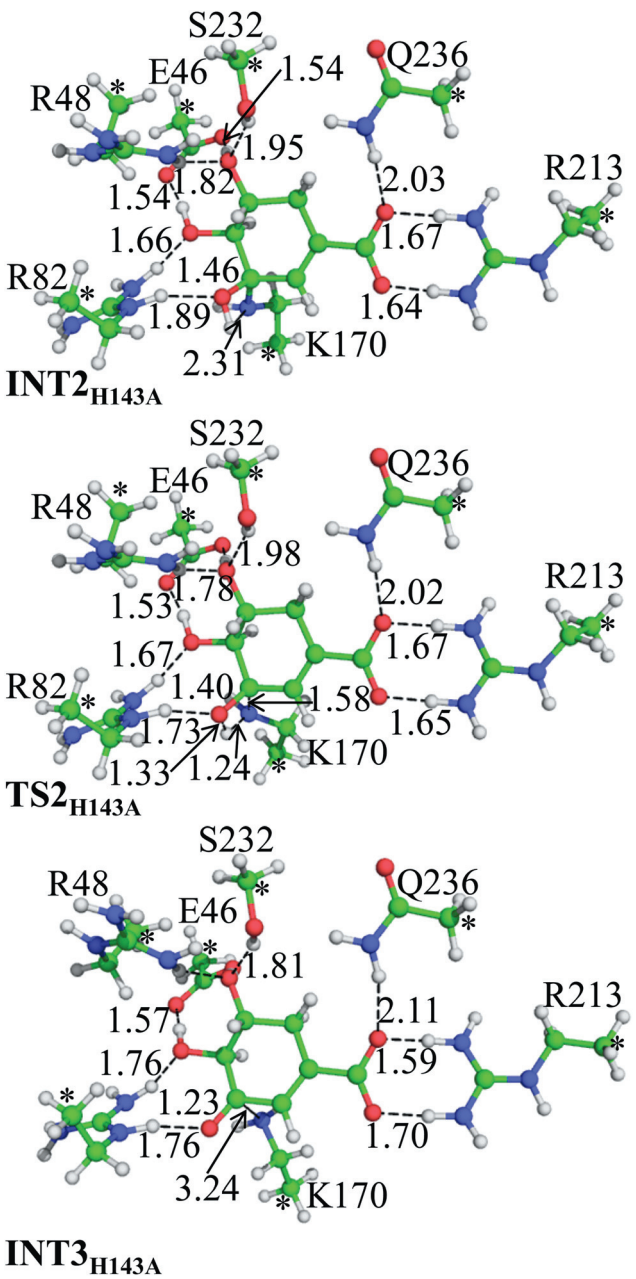

Fig. 5 The optimized geometries in the second reaction step of the H143A mutant.

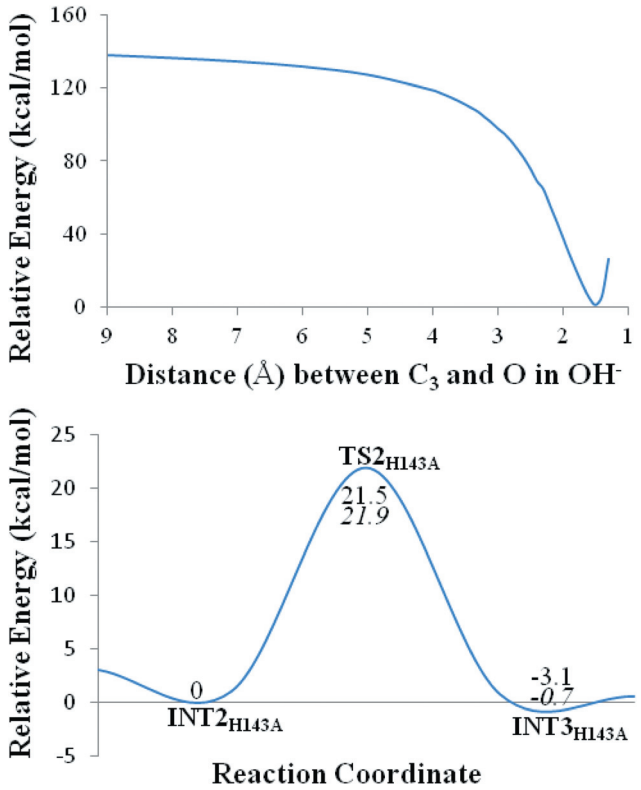

Fig. 6 The potential energy curve for nucleophilic attack on theC_3 atom by hydroxide ion (top) and the potential energy profile of the dissociation between the product and the Lys170 residue (bottom) in Schiff base hydrolysis catalyzed by the H143A mutant. The energies calculated in enzymatic environment are given in italic type.

reaction undergoes a two-step reaction pathway, including the barrierless nucleophilic attack on the C_3 atom by hydroxide ion and the dissociation between the product and the Lys170 residue through a four-membered ring transition state. The second step is determined to be the rate-determining step, consistent with the prediction on the basis of the kinetics result of the H143A mutant.[12] The calculated energy barrier of ~21.9 kcal mol^{-1} in enzymatic environment is also in good agreement with the activation free energy of ~24.0 kcal mol^{-1} derived from the experimental rate constant (K_{cat} = 4.5 × 10^{-4} s^{-1})[12] by using the conventional transition state theory (CTST).[45,46] Both the previous kinetics results[12] and our results presented here clearly show that the energy barrier increases remarkably without the catalytic role of His143 residue. Conclusively, both the reaction mechanism and the kinetics of the Schiff base hydrolysis are significantly changed by the H143A mutation and this result further demonstrates how a single amino-acid mutation on an enzyme can dramatically change both the reaction mechanism and the reaction rate.

A careful comparison between the reaction mechanisms of the Schiff base hydrolysis of wild-type type I DHQD and the H143A mutant also reveals some important and remarkable roles of the His143 residue during the reaction, as discussed below. Firstly, the His143 residue is a crucial factor for stabilizing the nucleophile water molecule through strong hydrogen bonding interaction. Secondly, His143 acts as a general base to accept a proton from the nucleophile water molecule in the first step, and the nucleophilic attack on the C_3 atom is therefore facilitated. Thirdly, through the deprotonation in the second step, the His143 residue acts as a general base once again to accept the proton in 3-hydroxyl group in the third step. Therefore, the steric hindrance caused by the direct proton transfer from the 3-hydroxyl group to the NZ atom in the Lys170 residue is avoided. Overall, the catalytic role of the His143 residue is more complicated than the previously proposed one shown in Scheme 2.

Conclusion

The fundamental reaction mechanism for the hydrolysis of the Schiff base intermediate has been studied by performing MD simulations and quantum chemical calculations. The detailed reaction pathway has been elucidated and it is different from the previously proposed one. First, a nucleophilic attack on the C_3 atom of the Schiff base intermediate is carried out by the water oxygen atom, and this step is facilitated by the His143 residue as a general base through a proton transfer from the water molecule to the $N^{\varepsilon 2}$ atom of the His143 residue. Then, the His143 residue is deprotonated through a proton transfer to the NZ atom of the Schiff base intermediate. Finally, the covalent bond between the product and the Lys170 residue breaks and the Schiff base intermediate is completely hydrolyzed. This process is also facilitated by the His143 residue through absorbing the proton in 3-hydroxyl group in the Schiff base intermediate. During the reaction process, His143 residue acts as a general base twice to facilitate the hydrolysis of the Schiff base intermediate. By comparison with our recently reported results on the Schiff base formation and dehydration process, it can be concluded that the hydrolysis of the Schiff base intermediate is the rate-determining step in the overall dehydration reaction of dehydroquinate catalyzed by type I DHQD, which confirms the prediction that the hydrolysis of the Schiff base intermediate is the rate-determining step. The calculated energy barrier of ~16.0 kcal mol^{-1} is in good agreement with the experimentally derived activation free energy of ~14.3 kcal mol^{-1}. The effects on the reaction by missing the imidazole group of His143 residue have also been studied and the Schiff base hydrolysis found to be initiated by hydroxide ion in the solution, rather than water molecule and both the reaction mechanism and the kinetics are significantly changed. This provides computational evidence for the important role of the His143 residue during the reaction.

Like all catalysts, enzymes increase the chemical reaction rate by stabilizing a high-energy transition state intermediate which lowers the activation energy of the reaction. Transition state analogs that mimic this high-affinity intermediate but that do not undergo the catalyzed chemical reaction can therefore bind much stronger to an enzyme than simple substrate or product analogs.[47] The theory for tight binding of transition state analogs has been supported by natural product chemistry and synthetic states[48,49] and has been successfully used to design high-activity inhibitors.[50–52] Based on the detailed reaction mechanism of the dehydration of dehydroquinate catalyzed by type I DHQD in the present study, future efforts aimed at designing high-activity inhibitors of type I DHQD should focus on the transition state involved in the rate-determining step, the second step, of the

Schiff base hydrolysis. This transition state has the highest energy and the analogs of this transition state may have very high activity at inhibiting the enzymatic activity. Thus, the new mechanistic insights in the present study will be very valuable for the future rational design of inhibitors of type I DHQD as non-toxic antimicrobials, anti-fungals, and herbicides.

Acknowledgements

This work was supported by the Major State Basic Research Development Programs of China (2011CBA00701, 2012CB721003), the National Natural Science Foundation of China (20973049), Open Project of State Key Laboratory of Urban Water Resource and Environment (No. QA201120), the Fundamental Research Funds for the Central Universities (Grant No. HIT.NSRIF.2013056), and Development Program for Outstanding Young Teachers (Grant No. HITQNJS.2009.069) in Harbin Institute of Technology.

References

1 R. Bentley, *Crit. Rev. Biochem. Mol. Biol.*, 1990, **25**, 307–384.
2 N. H. Giles, C. W. Partridge, S. I. Ahmed and M. E. Case, *Proc. Natl. Acad. Sci. U. S. A.*, 1967, **58**, 1930–1937.
3 D. A. Elsemore and L. N. Ornston, *J. Bacteriol.*, 1995, **177**, 5971–5978.
4 G. J. Euverink, G. I. Hessels, J. W. Vrijbloed, J. R. Coggins and L. Dijkhuizen, *J. Gen. Microbiol.*, 1992, **138**, 2449–2457.
5 J. R. Butler, W. L. Alworth and M. J. Nugent, *J. Am. Chem. Soc.*, 1974, **96**, 1617–1618.
6 D. G. Gourley, A. K. Shrive, I. Polikarpov, T. Krell, J. R. Coggins, A. R. Hawkins, N. W. Isaacs and L. Sawyer, *Nat. Struct. Biol.*, 1999, **6**, 521–525.
7 C. Kleanthous, R. Deka, K. Davis, S. M. Kelly, A. Cooper, S. E. Harding, N. C. Price, A. R. Hawkins and J. R. Coggins, *Biochem. J.*, 1992, **282**, 687–695.
8 P. J. White, J. Young, I. S. Hunter, H. G. Nimmo and J. R. Coggins, *Biochem. J.*, 1990, **265**, 735–738.
9 J. M. Harris, C. Gonzalez-Bello, C. Kleanthous, A. R. Hawkins, J. R. Coggins and C. Abell, *Biochem. J.*, 1996, **319**(Pt 2), 333–336.
10 K. R. Hanson and I. A. Rose, *Proc. Natl. Acad. Sci. U. S. A.*, 1963, **50**, 981–988.
11 J. Harris, C. Kleanthous, J. R. Coggins, A. R. Hawkins and C. Abell, *J. Chem. Soc., Chem. Commun.*, 1993, 1080–1081.
12 A. P. Leech, R. James, J. R. Coggins and C. Kleanthous, *J. Biol. Chem.*, 1995, **270**, 25827–25836.
13 C. A. Bonner and R. A. Jensen, *Biochem. J.*, 1994, **302**(Pt 1), 11–14.
14 S. Chaudhuri, K. Duncan, L. D. Graham and J. R. Coggins, *Biochem. J.*, 1991, **275**(Pt 1), 1–6.
15 R. K. Deka, C. Kleanthous and J. R. Coggins, *J. Biol. Chem.*, 1992, **267**, 22237–22242.
16 J. D. Moore, A. R. Hawkins, I. G. Charles, R. Deka, J. R. Coggins, A. Cooper, S. M. Kelly and N. C. Price, *Biochem. J.*, 1993, **295**(Pt 1), 277–285.
17 C. Kleanthous, M. Reilly, A. Cooper, S. Kelly, N. C. Price and J. R. Coggins, *J. Biol. Chem.*, 1991, **266**, 10893–10898.
18 A. Reilly, P. Morgan, K. Davis, S. M. Kelly, J. Greene, A. J. Rowe, S. E. Harding, N. C. Price, J. R. Coggins and C. Kleanthous, *J. Biol. Chem.*, 1994, **269**, 5523–5526.
19 S. H. Light, G. Minasov, L. Shuvalova, M. E. Duban, M. Caffrey, W. F. Anderson and A. Lavie, *J. Biol. Chem.*, 2011, **286**, 3531–3539.
20 W. H. Lee, L. A. Perles, R. A. P. Nagem, A. K. Shrive, A. Hawkins, L. Sawyer and I. Polikarpov, *Acta Crystallogr., Sect. D: Biol. Crystallogr.*, 2002, **58**, 798–804.
21 C. E. Nichols, M. Lockyer, A. R. Hawkins and D. K. Stammers, *Proteins*, 2004, **56**, 625–628.
22 N. N. Smith and D. T. Gallagher, *Acta Crystallogr., Sect. F: Struct. Biol. Cryst. Commun.*, 2008, **64**, 886–892.
23 Y. Yao and Z.-S. Li, *Chem. Phys. Lett.*, 2012, **519–520**, 100–104.
24 Q. Pan, Y. Yao and Z.-S. Li, *Theor. Chem. Acc.*, 2012, **131**, 1204.
25 D. A. Case, T. E. Cheatham, T. Darden, H. Gohlke, R. Luo, K. M. Merz, A. Onufriev, C. Simmerling, B. Wang and R. J. Woods, *J. Comput. Chem.*, 2005, **26**, 1668–1688.
26 T. A. Case Dad, T. E. Cheatham, C. L. Simmerling, J. Wang, R. E. Duke, R. Luo, K. M. Merz, D. A. Pearlman, M. Crowley, R. C. Walker, W. Zhang, B. Wang, S. Hayik, A. Roitberg, G. Seabra, K. F. Wong, F. Paesani, X. Wu, S. Brozell, V. Tsui, H. Gohlke, L. Yang, C. Tan, J. Mongan, V. Hornak, G. Cui, P. Beroza, D. H. Mathews, C. Schafmeister, W. S. Ross and P. A. Kollman, *Amber 9*, University of California, San Francisco, 2006.
27 W. L. Jorgensen, J. Chandrasekhar, J. D. Madura, R. W. Impey and M. L. Klein, *J. Chem. Phys.*, 1983, **79**, 926–935.
28 S. Miyamoto and P. A. Kollman, *J. Comput. Chem.*, 1992, **13**, 952–962.
29 J. P. Ryckaert, G. Ciccotti and H. J. C. Berendsen, *J. Comput. Phys.*, 1977, **23**, 327–341.
30 M. J. T. Frisch, G. W. Trucks, H. B. Schlegel, G. E. Scuseria, M. A. Robb, J. R. Cheeseman, J. J. A. Montgomery, T. Vreven, K. N. Kudin, J. C. Burant, J. M. Millam, S. S. Iyengar, J. Tomasi, V. Barone, B. Mennucci, M. Cossi, G. Scalmani, N. Rega, G. A. Petersson, H. Nakatsuji, M. Hada, M. Ehara, K. Toyota, R. Fukuda, J. Hasegawa, M. Ishida, T. Nakajima, Y. Honda, O. Kitao, H. Nakai, M. Klene, X. Li, J. E. Knox, H. P. Hratchian, J. B. Cross, V. Bakken, C. Adamo, J. Jaramillo, R. Gomperts, R. E. Stratmann, O. Yazyev, A. J. Austin, R. Cammi, C. Pomelli, J. W. Ochterski, P. Y. Ayala, K. Morokuma, G. A. Voth, P. Salvador, J. J. Dannenberg, V. G. Zakrzewski, S. Dapprich, A. D. Daniels, M. C. Strain, O. Farkas, D. K. Malick, A. D. Rabuck, K. Raghavachari, J. B. Foresman, J. V. Ortiz, Q. Cui, A. G. Baboul, S. Clifford, J. Cioslowski, B. B. Stefanov, G. Liu, A. Liashenko, P. Piskorz, I. Komaromi, R. L. Martin, D. J. Fox, T. Keith, M. A. Al-Laham, C. Y. Peng, A. Nanayakkara, M. Challacombe, P. M. W. Gill, B. Johnson, W. Chen, M. W. Wong, C. Gonzalez and J. A. Pople, *GAUSSIAN 03, (Revision E.01)*, Gaussian, Inc., Wallingford CT, 2004.
31 M. Cossi, V. Barone, R. Cammi and J. Tomasi, *Chem. Phys. Lett.*, 1996, **255**, 327–335.
32 S. Miertus, E. Scrocco and J. Tomasi, *Chem. Phys.*, 1981, **55**, 117–129.
33 S. Miertus and J. Tomasi, *Chem. Phys.*, 1982, **65**, 239–245.
34 L. Noodleman, T. Lovell, W. G. Han, J. Li and F. Himo, *Chem. Rev.*, 2004, **104**, 459–508.
35 F. C. Cui, X. L. Pan and J. Y. Liu, *J. Phys. Chem. B*, 2010, **114**, 9622–9628.
36 F. Himo, S. L. Chen, T. Marino, W. H. Fang and N. Russo, *J. Phys. Chem. B*, 2008, **112**, 2494–2500.
37 F. Himo, R. Z. Liao and J. G. Yu, *Proc. Natl. Acad. Sci. U. S. A.*, 2010, **107**, 22523–22527.
38 F. Himo, R. Z. Liao and J. G. Yu, *J. Phys. Chem. B*, 2010, **114**, 2533–2540.
39 R. Z. Liao, J. G. Yu and F. Himo, *J. Chem. Theory Comput.*, 2011, **7**, 1494–1501.
40 F. C. Cui, X. L. Pan, W. Liu and J. Y. Liu, *J. Comput. Chem.*, 2011, **32**, 3068–3074.
41 J. Wang, J. Gu and J. Leszczynski, *J. Phys. Chem. B*, 2008, **112**, 3485–3494.
42 J. Wang, J. Gu, J. Leszczynski, M. Feliks and W. A. Sokalski, *J. Phys. Chem. B*, 2007, **111**, 2404–2408.
43 Y. Zhang, D. Chen, H. Zhang, J. Liu, S. Mi and G. Zhang, *Int. J. Quantum Chem.*, 2012, **112**, 889–899.
44 S. Sharma and P. Bandyopadhyay, *J. Mol. Model.*, 2012, **18**, 481–492.
45 J. R. Alvarez-Idaboy, A. Galano, G. Bravo-Pérez and M. E. Ruiz, *J. Am. Chem. Soc.*, 2001, **123**, 8387–8395.
46 D. G. Truhlar and B. C. Garrett, *Annu. Rev. Phys. Chem.*, 1984, **35**, 159–189.
47 V. L. Schramm, *J. Biol. Chem.*, 2007, **282**, 28297–28300.
48 R. Wolfenden, *Acc. Chem. Res.*, 1972, **5**, 10–18.
49 R. Wolfenden, *Biophys. Chem.*, 2003, **105**, 559–572.
50 V. L. Schramm, *Annu. Rev. Biochem.*, 2011, **80**, 703–732.
51 V. L. Schramm and P. C. Tyler, *Iminosugars*, John Wiley & Sons Ltd, 2008, pp. 177–208.
52 T. L. Amyes and J. P. Richard, *ACS Chem. Biol.*, 2007, **2**, 711–714.

